# Coordinated control approach for load following operation of SOFC-GT hybrid system

Xusheng Wang[1], Xiaojing Lv*[,2], Catalina Spataru[3], Yiwu Weng*[,1]

[1] Key Laboratory for Power Machinery and Engineering of Ministry of Education, School of Mechanical Engineering, Shanghai Jiao Tong University, Shanghai, 200240, China

[2] China-UK Low Carbon College, Shanghai Jiao Tong University, Shanghai, 201306, China

[3] Energy Institute, University College London, 14 Upper Woburn Place, London, WC1H 0NN, UK

**Abstract:** A novel control approach which combined the multi control loops with the coordinated protection loops is designed in this paper to address the fast load following, ensure safe and high efficiently operation of SOFC-GT. The fuzzy PID controller is developed to meet the control requirements of the nonlinear time varying SOFC-GT hybrid system. The analysis in system transient behavior during load step changes operation reveal that the designed coordinated control structure can realize parameters decoupling and eliminate the instability of SOFC-GT in the process of power tracking. The maximum current overshoot is decreased from 18.2% to 7.4% while the temperature control and current changing rate coordinated control are enabled together in the load step-down operation. Which causes the transient maximum temperature changing rate is decreased by almost 47.7%. The results also indicated that the temperature overshoot is reduced from 2.28% to 1.12% while the air flow rate coordinated control and temperature gradient coordinated control are enabled together in the load step-up operation, which leads to the transient maximum temperature gradient is decreased by almost 0.18K/cm.

**Key words:** Solid oxide fuel cell, Gas turbine, Load following, Hybrid system, Coordinated control.

## 1. Introduction

At present, energy shortages and environmental deterioration have become major threats to sustainable development. According to the forecasts from EIA (Energy Information Administration), the world energy consumption has been estimated to increase nearly 50% between 2018 and 2050[1]. Hence, it is urgently need to develop more efficient power generation technologies to cover the energy demand in mid-term future and to support the transition to net zero. Solid oxide fuel cell (SOFC) could play a key role due to potential

* Corresponding authors.

E-mail addresses: lvxiaojing@sjtu.edu.cn (X. Lv), ywweng@sjtu.edu.cn (Y. Weng).

to achieve a high system efficiency for electricity generation [2]. In addition, because of the high operation temperature of SOFC (up to 1000℃[3]), it can be easily integrated with gas turbine to improve the power generation efficiency[4-5]. A comparison among different technologies (Fig.1) show that the electrical efficiency is raised obviously by combined the SOFC and gas turbine together. The electrical efficiency of SOFC-GT is in the range of 60-70%[6-7], which makes such hybrid systems as one of the most promising power generation technologies.

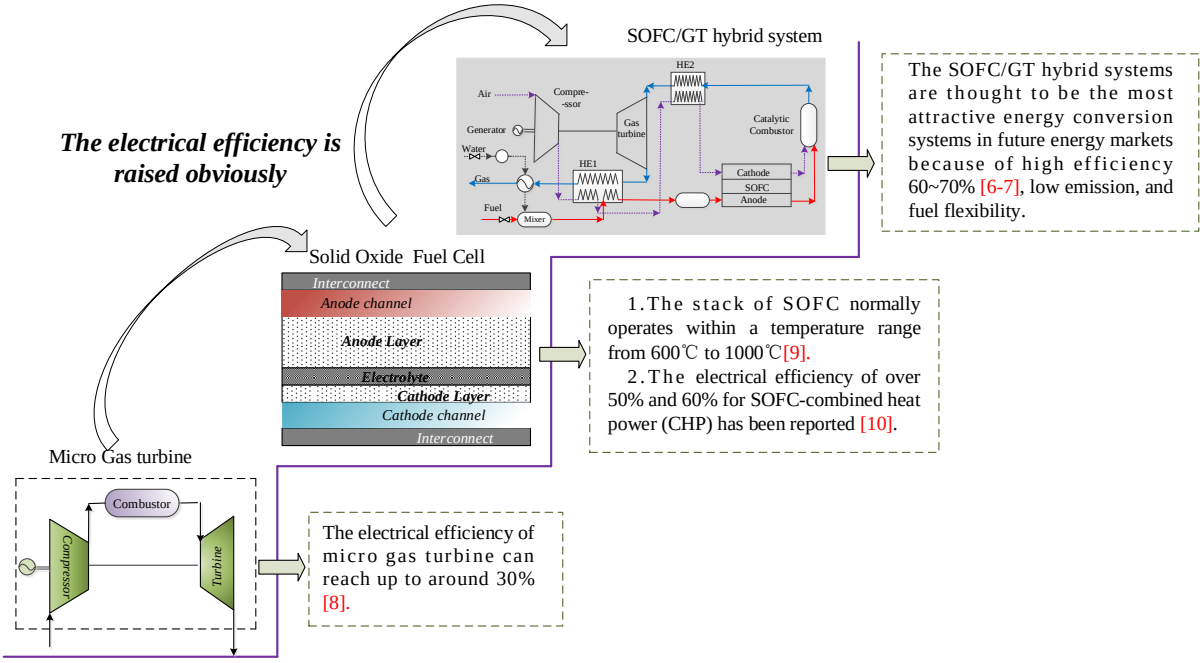


Fig.1 Comparison among different technologies

The SOFC-GT hybrid system show several benefits: high electrical efficiency, lower greenhouse gas emissions. It can be used to produce concentrated $CO_2$ for sequestration by simply cooling the anode exhaust of SOFC[11]. In recent years, the research about SOFC-GT mainly focus on configuration, off-design operation, thermal management, transient behaviors, control strategies and hardware-in-the-loop simulation [12]. For SOFC-GT hybrid systems, various parameters, such as, fuel flow rate, stacks current, fuel utilization, turbine inlet temperature and steam to carbon ratio, are strongly coupled with each other to influence the system performance. The complex operation characteristics of highly nonlinear, time-varying, large time delay and strong coupling among components of the hybrid system bring new challenges to coordinate control and safety operation. Although the variable GT speed strategy results in a more efficient control effect for the temperature control of SOFC-GT[13], the compressor might easily to surge when the air flow rate or rotate speed of compressor deviation too much from the expected values. In the aspects of power tracking, the current is generally selected as the manipulated variable for power control[14]. However, a big load change may easily lead to a sharply change in SOFC current, with negative impacts for the hybrid system when protection control loops are not enabled. Meanwhile, constant fuel utilization (FU)

control is usually used in SOFC-GT by adjusting the fuel flow rate. How to select the reasonable set point of FU in transient process brings new challenges for the design of control system. According to a report from Akkaya[15] that the highest efficiency occurs at 75% FU for a methane fueled pressurized SOFC-GT. Danylo has investigated the influence of FU on the performance of SOFC-GT, results indicate that the electrical efficiency higher than 70% can be achieved over a wide ranges of fuel utilization (60%-90%)[16].

Current, study on control strategies for SOFC-GT have been involved in many research aspects. A control structure with PI controllers is designed by Kandepu for the SOFC-GT based power system to compensate the load disturbances. The fuel utilization and SOFC temperature are taken as controlled variables in this study. Results concluded that the efficiency of the system is decreased with the use of blow-off to control the SOFC temperature[17]. A control approach based on feed-forward and standard proportional-integral techniques is suggested by Ferrari[18] to avoid failures and stress conditions detrimental to component life. Results indicated that the proposed control approach can minimize the maximum temperature gradient inside the fuel cell, reduce the pressure gap between cathode and anode sides and generate a higher safe margin for steam to carbon ratio. Chen performed a multi-loop control strategy for a hybrid SOFC-GT system based on the conventional PID controller[19], the control variables in this work involves power, FU, SOFC temperature, TIT and rotation speed of gas turbine.

Although the PID controller has been widely used in industrial control due to its simple structure, fast response and high accuracy. For the nonlinear time-varying system, the conventional PID controller is relatively inefficient to provide an appropriate level of flexibility and performance in different operating conditions due to the constant control coefficients during the time [20]. The advanced control methods have been reported to address the nonlinear control problems in SOFC hybrid systems. A fuzzy-PD controller is developed by Marzooghi[21] to solve the performance degradation of SOFC systems in micro grids under voltage flicker, the results shown that a satisfactory control effect is obtained while the fuzzy-PI controller is started. A multivariable multi-loop feedforward/feedback control structure based on robust PID controller is designed for a kW-scale solid oxide fuel cell by Cao[22], in which a feedforward control structure was designed based on the stack current and a feedback controller was implemented by a single neuron adaptive PID algorithm. The results show that this control structure has well robustness and stability for the SOFC system.

Although the advanced control methods have been reported by several literatures to address the problems in transient process of SOFC-GT hybrid system, most of which without design the reasonable protection loops to coordinate control the hybrid SOFC-GT systems in real time. And the key parameters of hybrid SOFC-GT system will easily exceed the safe limit during load big changes, which might permanently damage the components of hybrid system. Meanwhile, many studies ignore the transient behavior of maximum temperature changing rate and

maximum temperature gradient inside fuel stacks[22]. However, high temperature gradient or rapid transient changing may cause the excessive thermal stresses within the fuel cell, leading to cell breakdown. Furthermore, a several studies select the average temperature in SOFC or the inlet temperature at anode channel as the control variables[19,23], there are very few reports focus on the transient behavior of maximum temperature.

Based what is discussed above, a control approach combined the multi control loops with the coordinated protection loops is proposed in this paper, meanwhile, the fuzzy PID controller is developed to meet the control requirements of the nonlinear time varying SOFC-GT hybrid system. The control loops in this work involves power control, temperature control, fuel utilization control and steam to carbon control. The maximum temperature inside fuel stacks is selected as control variable in the temperate control. The protection loops are used to coordination control the SOFC-GT hybrid system in real-time, with focus on the safety margin of the following parameters: compressor surge, turbine inlet temperature, transient temperature changing rate and temperature gradient inside fuel cell stacks. In addition, the variation ranges of maximum temperature at PEN (positive-electrode/electrolyte/negative-electrode) structure, output power and electrical efficiency of the hybrid system are investigated, which can give instructions to determine the set point of temperature for temperature controller. Also, an in-depth analysis in system transient behavior during load step changes operation is conducted to exhibit the performance of load following of SOFC-GT.

Nomenclature

| | | | |
|---|---|---|---|
| $A$ | Area ($m^2$) | *WGSR* | Water gas shift reaction |
| $a$ | Heat transfer coefficient ($W\ m^{-2}\ K^{-1}$) | $x$ | Axial coordinate (m) |
| $C$ | Heat capacity ($J\ K^{-1}$) | Greek symbols | |
| $c_p$ | Specific heat capacity ($J\ mol^{-1}\ K^{-1}$) | $\Delta H$ | Enthalpy change of reaction ($J\ mol^{-1}$) |
| $d$ | Hydraulic diameter of channel (m) | $\Delta t$ | Sample time (s) |
| $E$/ $E_a$ | Activation energy($J\ mol^{-1}$) | $\Delta T/\Delta t$ | Temperature changing rate (K/s) |
| $F$ | Faraday constant ($C\ mol^{-1}$) | $\Delta T/\Delta x$ | Temperature gradient (K/cm) |
| $J$ | Average current density ($A\ m^{-2}$) | $\varepsilon$ | Coordination factor |
| $h$ | Channel height (m)<br>Specific enthalpy ($J\ mol^{-1}$) | $\rho$ | Density ($g\ m^{-3}$) |
| $K$ | Equilibrium constant | $\eta$ | Polarization(V)<br>Electrical efficiency |
| $k$ | Pre-exponential constant ($mol\ s^{-1}\ m^{-1}\ bar^{-1}$)<br>Heat transfer coefficient ($J\ m^{-2}\ s^{-1}\ K^{-1}$) | $\lambda$ | Heat conductivity ($J\ m^{-1}\ s^{-1}\ K^{-1}$) |
| $M$ | Mass (g) | $\tau$ | Thickness (m) |
| $m_{fuel}$ | Fuel flow rate ($mol\ s^{-1}$) | Subscripts | |
| *MSR* | Methane-steam reforming | a | Air channel |
| $n$ | Mole flow rate ($mol\ s^{-1}$) | act | Activation polarization |
| $Nu$ | Nusselt number | cc | Catalytic combustor |
| $P$ | Pressure (bar) | conc | Concentration polarization |
| $p$ | Partial pressure of spices | ele | Electrochemical reaction |

| | | | |
|---|---|---|---|
| $Q$ | Heat (J) | f | Fuel channel |
| $q_{radiative}$ | Radiation heat transfer (J $m^{-2}$ $s^{-1}$) | I | Interconnect |
| $R$ | Gas constant (J $mol^{-1}$ $K^{-1}$)<br>Rate of reaction (mol $m^{-2}$ $s^{-1}$) | in | Inlet |
| $T$ | Temperature (K) | ohm | Ohm polarization |
| $t$ | Time (s) | out | Outlet |
| $U$ | Cell potential (V) | PEN | PEN structure |
| $u$ | Velocity (m $s^{-1}$) | re | Pre-reformer |

## 2. System description

A 242kW SOFC-GT hybrid system fueled by methane is designed in this work, and Fig.2 illustrates the schematic diagram of the solid oxide fuel cell-gas turbine (SOFC-GT) hybrid system. The hybrid system mainly involves a micro gas turbine (MGT), a direct internal reforming solid oxide fuel cell (DIR-SOFC), a catalytic combustor, a pre-reformer, several heat exchangers and other components. The air (State1) is firstly pressurized by the compressor. Then, the compressed air (State2) flow through HE2 and HE3 successively before it enters the cathode channel of SOFC. Meanwhile, the methane (State8) is mixed with the steam (State7) in the mixer, and then the mixed fuel (State 9) is heated at HE1 before it enters the pre-reformer. Also, the water is firstly pressurized and then vaporized before it enters the mixer. In the pre-reformer, a small part of methane is reacted with the steam to produce $H_2$ and $CO_2$. After the process of pre-reforming, the gas (State11) flow through the anode channel of SOFC to provide hydrogen for electrochemical reaction. The gas contains the unreacted fuel from anode channel (State12) and the excess air from cathode channel (State5) are further burnt in the catalytic combustor. Finally, the heat is carried by turbine exhaust (State15) is recovered by the feed fuel, air and water successively.

For the configuration of SOFC-GT, most researches report a high-temperature heat exchanger before turbine inlet [24]. Because both the gas flow rate and the temperature difference between high temperature gas and turbine working temperature in small size gas turbines are relatively smaller, a ceramic heat exchanger with low effectiveness is installed between turbine and combustor is acceptable. Traverso [26] has proved the practicability and feasibility of this configuration for SOFC-GT. Although the present capital cost of such kind SOFC-GT systems is relatively high, estimated is 7.25 k€/kW in case of mass production according to a report from Consultant RBS [27], the higher electrical efficiency (up to 70%) makes the SOFC-GT is regarded as a promising power generation technology in future [8].

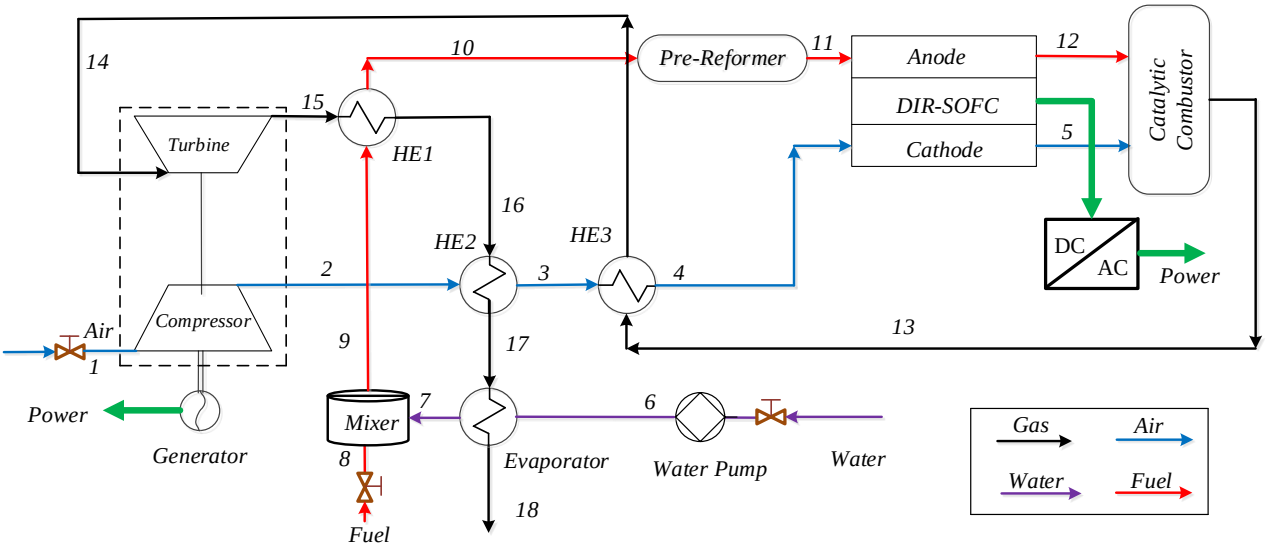


Fig.2. Configuration of SOFC-GT hybrid system

The key parameters of the SOFC-GT hybrid system are specified in Table.1.

Table.1. Parameters specification of SOFC-GT hybrid system [28-31].

| Parameters | Value | Unit |
|---|---|---|
| Air compressor ratio | 3.76 | - |
| Steam to carbon ratio | 2 | - |
| SOFC average current density | 4000 | $A/m^2$ |
| Rotate speed of MGT | 96000 | r/min |
| SOFC operation pressure | 3.68 | bar |
| Cell potential | 0.626 | V |
| Fuel utilization of cell | 0.75 | - |
| Anode thickness | 0.5 | mm |
| Cathode thickness | 0.05 | mm |
| Electrolyte thickness | 0.02 | mm |
| Cell stack length | 0.4 | m |
| Cell stack width | 0.1 | m |
| Output power of SOFC-GT | 242 | kW |

## 3. Mathematical model

### 3.1 Solid Oxide Fuel Cell

The methane is firstly reformed with steam in the pre-reformer before it is fed to the fuel channel of DIR-SOFC to provide hydrogen for electrochemical reaction. The synthesis gas at the anode inlet mainly contains methane, steam and a small amount of carbon dioxide, carbon monoxide and hydrogen. In the methane-fueled SOFC, the methane is directly reformed in anode layer to provide $H_2$ and CO on the surface of the catalyst particles[32]. And the CO can be further reacted with steam to produce $H_2$ and $CO_2$ in the fuel channel[33]. The

schematic diagram of a planar SOFC and computation domain are shown in Fig.3, including fuel channel, air channel, two interconnectors, and electrochemically active tri-layer consists of porous anode, electrolyte and porous cathode (PEN structure). The cell size and component thickness are used in this study from the model developed by Aguiar[34], a unit planar SOFC comprising four single cells in series, each of 10cm×10 cm[35]. The SOFC model development in this paper mainly focuses on electrochemical principles, mass and energy balances.

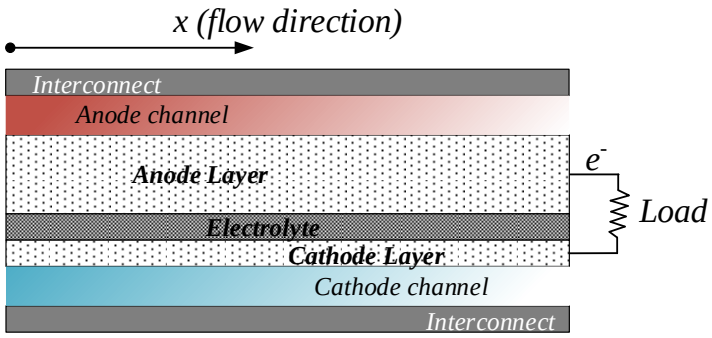


Fig.3. Computational domain of a unit planar SOFC

3.1.1 Mass and energy balances

For the SOFC stacks with direct internal reforming, the species in the fuel channel involves $CH_4$, $H_2O$, CO, $H_2$, and $CO_2$. The steam reforming reaction (Eq.1) and the gas shift reaction (Eq.2) are occurred in the anode catalyst layer[33].

$$CH_4+H_2O \leftrightarrow CO+3H_2 \quad (1)$$

$$CO+H_2O \leftrightarrow CO_2+H_2 \quad (2)$$

Reactions of steam reforming and gas shift provide sufficient hydrogen for fuel cell stacks. The hydrogen is oxidized in the anode side to generate electrons, meanwhile, the oxygen is reacted with electrons in the cathode side to generate oxygen ions. And the useful work is produced in the process of transport electrons from the anode side to the cathode side via an external circuit. It should be noted that, the electrochemical reaction of CO in fuel cell stacks is generally neglected due to the carbon monoxide electrochemical oxidation velocity is 2-5 times slower than that of hydrogen [36]. The electrochemical reaction between hydrogen and oxygen inside the cell are shown as follow:

$$\text{Anode:}\quad H_2+O^{2-} \rightarrow H_2O+2e^- \quad (3)$$

$$\text{Cathode:}\quad \frac{1}{2}O_2+2e^- \rightarrow O^{2-} \quad (4)$$

$$\text{Overall reaction:}\quad H_2+\frac{1}{2}O_2 \rightarrow H_2O \quad (5)$$

The dynamic species concentrations in fuel and air channel are mainly determined by the local current density and the kinetic rates of reforming reactions. The reaction of methane-steam reforming (SMR) is assumed occurs at

a finite rate, and can be give as[38]:

$$R_{MSR} = k_0 p_{CH_4} \exp\left(-\frac{E_a}{RT}\right) \tag{6}$$

Where, $k_0$ is a pre-exponential constant, $p_{CH4}$ is the partial pressure of methane, $E_a$ is an activation energy, $R$ is gas constant, $T$ is reaction temperature. Meanwhile, the reaction of water gas shift (WGSR) is considered to be occurred at chemical equilibrium conditions[39]. The equilibrium constant of WGSR can be obtained as:

$$K_{WGSR} = \frac{p_{H_2} p_{CO_2}}{p_{H_2O} p_{CO}} \tag{7}$$

Where, $p_i$ is the partial pressure of different spices.

The rate of electrochemical reaction is given according to Faraday's law:

$$R_{ele} = \frac{J}{2F} \tag{8}$$

Where, $J$ and $F$ are current density and Faraday constant respectively.

The reaction of electrochemical and the process of directly internal reforming are strongly coupled to influence the thermal management inside fuel cell stacks. The SMR is a strong endothermic reaction and the WGSR is a weak exothermic. Meanwhile, the electrochemical reaction release lot of heat. Besides, both the in-plane heat conduction through cell components and the convective heat transfer between cell components and fuel and air are strongly coupled. It is assumed that the current density to be uniform within the SOFC[40-41], meanwhile, it is considered that no heat flux through the external walls.

The energy conversion in anode channel can be give as follow[34]:

$$\rho_f c_{p.f} \frac{\partial T_f}{\partial t} = -u_f \rho_f c_{p.f} \frac{\partial T_f}{\partial x} + k_{f.PEN}(T_{PEN} - T_f)\frac{1}{h_f} + k_{f.I}\left(T_I - T_f\right)\frac{1}{h_f} + \sum\left(-\Delta H\right)_k R_k \frac{1}{h_f} \tag{9}$$

Where, the energy balances in anode channel involves convective heat transfer between fuel streams and solid part of fuel cell, and the reaction heat in the processes of internal reforming. The physical properties of gas, air and cell components in each control volumes are considered as the same. And $\Delta H$ means the enthalpy change of reaction MSR or WGSR; $x$ is the location along the flow direction.

Also, it is considered that the reaction enthalpies are released at the PEN structure[42], the energy balance equation in PEN structure can be obtained as follow[35]:

$$\begin{aligned}\rho_{PEN} c_{p.PEN} \frac{\partial T_{PEN}}{\partial t} = \lambda_{PEN} \frac{\partial^2 T_{PEN}}{\partial x^2} - k_{f.PEN}(T_{PEN} - T_f)\frac{1}{\tau_{PEN}} - k_{a.PEN}(T_{PEN} - T_a)\frac{1}{\tau_{PEN}} \\ + \left[-(\Delta H_{ele})R_{ele} - jU\right]\frac{1}{\tau_{PEN}} + q_{radiative}\frac{1}{\tau_{PEN}}\end{aligned} \tag{10}$$

Where, the energy balances in PEN structures involves convective heat transfer between are/fuel and PEN structure, reaction heat of hydrogen oxidation, generated power and radiation heat transfer. The boundary condition

of above equation is heat flux through the external walls is zero. The heat transfer coefficients in above equation were obtained based on a constant Nusselt number ($Nu$), given as follow[43]:

$$k = Nu\frac{\lambda_g}{d_h} \tag{11}$$

Where, the Nusselt number is assumed independent of the Reynolds number due to the laminar flow conditions [34]. λg is the heat conductivity of the gas mixture, $d_h$ means the channel hydraulic diameter.

3.1.2 Electrochemical reactions

The electrical potential of SOFC is a function of current density, gas composition and temperature. The theoretical open-circuit potential of fuel cell can be obtained by Nernst equation (Eq.12). However, due to the existing losses, the potential of fuel cell is always less than the theoretical open-circuit potential, written as Eq.13. In Eq.13, $\eta_{act}$, $\eta_{ohm}$ and $\eta_{con}$ represent activation overpotentials, ohmic loss and concentration overpotentials respectively.

$$E^{OCP}=E^{0}+\frac{RT}{2F}\ln\left(\frac{P_{H_2}P_{O_2}^{0.5}}{P_{H_2O}}\right) \tag{12}$$

$$U=E^{OCP}-\eta_{act}-\eta_{ohm}-\eta_{con} \tag{13}$$

The activation overpotential is related to the rate of electrochemical reaction and involves anode and cathode activation overpotentials. The ohmic losses occurs due to the electrons flow through the anode layer, cathode layer and electrolyte. Because the electrochemical reaction occurs at the three-phase boundary. The concentration of hydrogen, oxygen and steam at the three-phase boundary are different from the figures at channel. The concentration overpotentials appear when mass transport effects hinder the electrode reaction. The detail models and parameters can be found in literatures [34-35] and in our previous researches[28-31]. The validation of SOFC models can be found in our previous research[31], which conducted the validation process by comparing the simulation results with experimental data from [44] in the working conditions of temperature and pressure are 800℃ and 1bar respectively. Which concluded the reasonable and acceptable of the built SOFC models.

## 3.2 Gas turbine

The gas turbine is consisted by a centrifugal compressor and a radial turbine. The pressure and isentropic efficiency of centrifugal compressor can be obtained by the reduced mass flow and the reduced rotational speed, which can be reflected by the characteristic maps of compressor. In this paper, the gas turbine model is established based on the gas turbine characteristic maps from a real micro gas turbine (MGT)[28], the detail parameters and models of gas turbine can be found in [28, 30]. Also, the characteristics of GT can be obtained according to the

similar principles while the design parameters are changed. Besides that, for the purpose of validation, a micro gas turbine has been developed and experimented in Jiangjin Turbocharger Plant, China[45], shown in fig.4. The experimental results concluded that the compressor isentropic efficiency is between 70% and 84%, and turbine isentropic efficiency is higher than 80% with a maximum close to 83%[31]. All of this proven the reasonable of the gas turbine model.

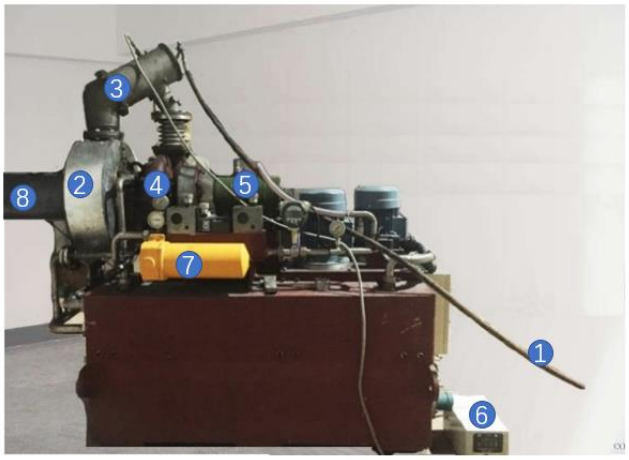


Micro gas turbine

PLC controller of MGT

1. Fuel intake pipe;2.Turbine; 3.Combustor;4.Compressor; 5. Generator; 6. Igniter; 7. Filter; 8. Exhaust

Fig.4. Micro gas turbine

## 3.3 Heat exchanger

The temperature of fluids is changed due to the heat transfer occurs in heat exchangers. The model of heat exchanger in this work is built according to the mass, momentum and energy balances[46], and the diagram of heat exchanger is shown in fig.5.

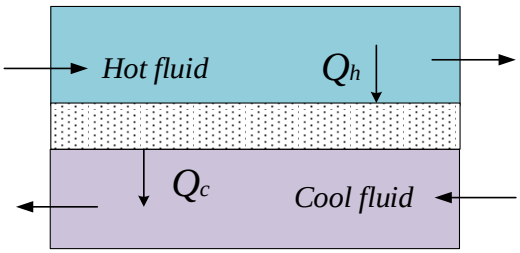


Fig.5. Scheme of heat exchanger

In Fig.5, $Q_c$ and $Q_h$ are the transferred heat between fluids and heat exchanger core, can be calculated as:

$$Q_h = a_h A_h \left( \frac{T_{h\_in} + T_{h\_out}}{2} - T_m \right) \tag{14}$$

$$Q_c = a_c A_c \left( T_m - \frac{T_{c\_in} + T_{c\_out}}{2} \right) \tag{15}$$

Where, $a_h$ and $a_c$ are the heat transfer coefficient of hot fluid and cool fluid respectively, $A_h$ and $A_c$ are the heat transfer area of hot side and cool side, $T_{\mathrm{m}}$ is the average temperature of heat exchanger core, given as:

$$c_m M_m \frac{dT_m}{dt} = Q_h - Q_c \tag{16}$$

Where, $c_m$ and $M_m$ are the specific heat and mass of heat exchanger core.

In addition, the detail models and descriptions about other component, such as reformer, catalytic combustor and mixer can be found in our previous studies [28-31]. To validate the feasibility of the combustion of SOFC anode exhaust, an experimental platform with the catalyst of 0.5%Pd/$ZrO_2$/g-$Al_2O_3$ was established in our previous research [47], the results concluded that the ultra-low heating value fuel from SOFC anode exhaust can be 100% utilized in catalytic combustor.

### 3.4 Operation boundary of SOFC-GT

The electrical potential of SOFC is increased with the raise in working temperature. However, the excessive working temperature might damage the materials permanently. Therefore, the working temperature of SOFC should be maintained in a reasonable range of 1023-1223K[48]. In addition, high temperature gradient or transient changing will cause the excessive thermal stresses within fuel cell stacks, leading to cell breakdown. It is reported that the excessive temperature gradient over 10K/cm[35] and temperature changing rate higher than 10K/min[49], which might damage the SOFC permanently. Also, the surge of compressor can lead to strong mechanical vibration and produce reverse flow of air, which will cause damage or fracture of the blades. To avoid the compressor surge, the minimum 12% of surge margin must be given in actual operation[30]. Also, the turbine inlet temperature (TIT) should be kept in a reasonable range to ensure the safely and efficiently operation of GT, and the maximum 1223K of TIT must be maintained for small size uncooled turbines[30].

## 4. Coordinated control

### 4.1. Fuzzy PID controller development

Previous studies have proven the excellent robustness, greater adaptability and strong anti-interference ability of fuzzy PID controller for the complex nonlinear time-varying systems[50]. This study builds on previous research by designing a fuzzy PID controller to adjust controller's coefficient The structure of fuzzy PID control is shown in Fig.6.

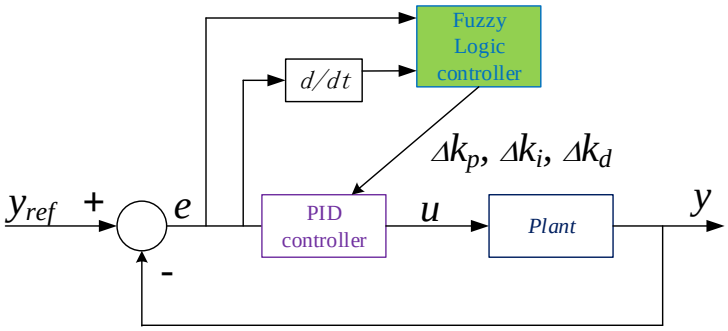


Fig.6. Structure of fuzzy PID controller

Clearly find that the input for the fuzzy PID controller is the deviation $e$ and the deviation rate $e_c$, meanwhile, the $k_p$, $k_i$ and $k_d$ are adjusted online according to the fuzzy inference rules. The input and output variables of the fuzzy inference were transformed into seven fuzzy variables [NB, NM, NS, ZO, PS, PM, PB] in the process of fuzzification. NB, NM, NS, ZO, PS, PM and PB denote negative big, negative medium, negative small, zero, positive small, positive medium and positive big respectively. The fuzzy controller is determined based on the membership functions and fuzzy rules, (Fig.7). Gaussian membership function is used for $e$ and $e_c$. Triangular membership function is used for $k_p$, $k_i$ and $k_d$ because uses less computation time[51].

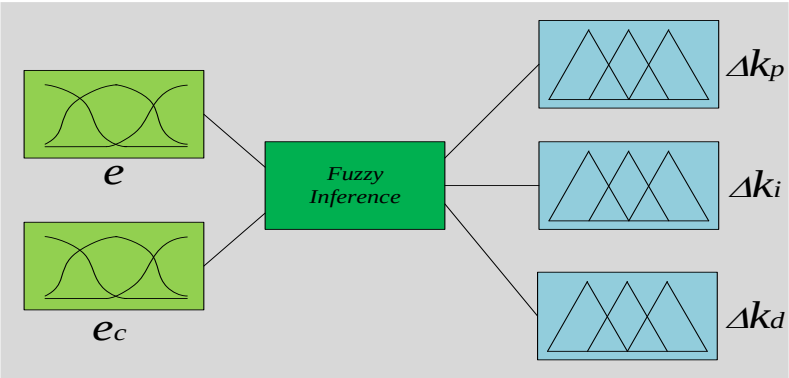


Fig.7.Structure of fuzzy controller

The control coefficients could be adjusted dynamically based on the fuzzy rules, and the formula of parameters self-tuning is given as follow[52]:

$$\begin{cases} k_p(t) = k_{p0} + \Delta k_p(t) \\ k_i(t) = k_{i0} + \Delta k_i(t) \\ k_d(t) = k_{d0} + \Delta k_d(t) \end{cases} \tag{17}$$

Where, $k_p$, $k_i$ and $k_d$ are the initial PID coefficients, and $\Delta k_p$, $\Delta k_i$ and $\Delta k_d$ are the three outputs of the fuzzy controller.

## 4.2 Control loops of SOFC-GT

The purpose of this experimental research is to adjust the hybrid SOFC-GT system to track the load safely,

efficiently and rapidly in the process of load following, meanwhile, regulating the fuel cell stacks temperature changes in a small range. The structure of multi control loops is given in Fig.8. The controlled variables (Fig 8) in this work involves of output power, maximum temperature at PEN structure, fuel utilization of SOFC and steam to carbon ratio, the manipulated variables are fuel cell stacks current, fuel flow rate, gas turbine rotate speed and water flow rate.

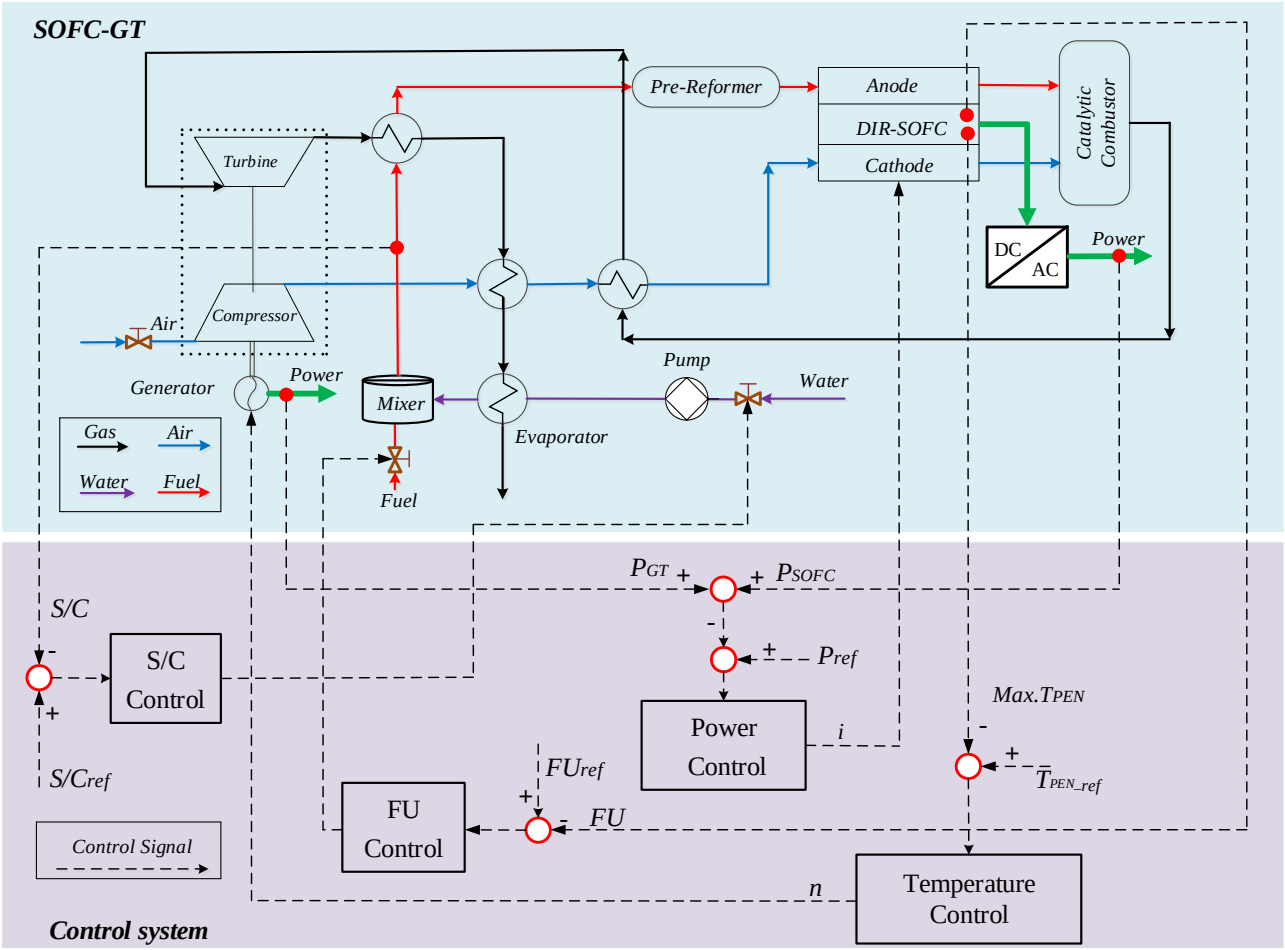


Fig.8. Control structure of SOFC-GT

- Power control: The output power of hybrid system should be flexibly adjusted to meet the load demand. The SOFC contributes most of the net power in the hybrid system[16], thus, this work manipulating the current of fuel cell stacks to follow the load. And this process can be done instantaneously by the power electronics[53].

- Temperature control: Although the system performance will be improved significantly while the working temperature of SOFC is increased, the fuel cell may occur thermal crack while the temperature is higher than the value of technological limit. For the purpose of safely and efficiently operation of SOFC-GT, the maximum temperature at PEN structure is controlled by manipulating the air flow rate. Generally, the air flow rate of SOFC-GT can be regulated by the rotate speed of micro gas turbine[23].

- Fuel utilization (FU) control: The FU has a strong influence on system electrical efficiency and working

temperature. A reasonable FU is one of the essential prerequisites to ensure the SOFC-GT operation safely and high efficiently. In this context, the constant FU control is the most used strategy for fuel control. The FU and current are coupled via the fuel flow rate, which can be obtained by the following equation:

$$FU = \frac{i / 2F}{(4y_{CH_4} + y_{H_2} + y_{CO})m_{fuel}} \tag{18}$$

where, $i$ is the current, F is the Faraday constant, $y$ represents the molar fraction of component, $m_{fuel}$ is the input fuel flow rate.

The FU is mainly related with the current of SOFC and the input fuel flow rate. Thus, this work keeps the fuel utilization constant by adjusting the fuel flow rate while the current is changed.

- Steam to carbon ratio (S/C) control: The steam is necessary in the process of reforming, a proper S/C can promote the production of hydrogen and inhibit the carbon deposition effectively. The critical value of S/C are directly determined by the reaction conditions[54-55]. Meanwhile, most studies so far have investigated that there is no carbon deposition taking place while the S/C is above 2 in the operation conditions of SOFC hybrid system[54]. The S/C can be given as:

$$S/C = \frac{m_{water}}{(y_{CH_4} + y_{CO_2} + y_{CO})m_{fuel}} \tag{19}$$

The S/C is directly depended on the input fuel and water flow rates. Therefore, this work maintains the S/C constant by manipulating the water flow rate while the fuel flow rate is changed.

## 4.3 Coordinated protection control

The SOFC-GT hybrid system has complex operation characteristics of highly nonlinear, time-varying, uncertainty and strong coupling. Also, the hybrid system with multiple controlled and manipulated variables. Although the fuzzy PID controller is beneficial to limit the system overshoot and shorten the transient behavior, the system not always satisfy its safety operation constraints only depend on the fuzzy controller. The key parameters of hybrid SOFC-GT hybrid will easily exceed the safe limit during load big changes, which causes the components of hybrid system damage permanently. Therefore, multi coordinated protection loops are performed in real time to realize parameters decoupling, eliminate the instability and ensure the safety operation in the transient process of SOFC-GT. The structure of the proposed coordinated control approach is given in Fig.9.

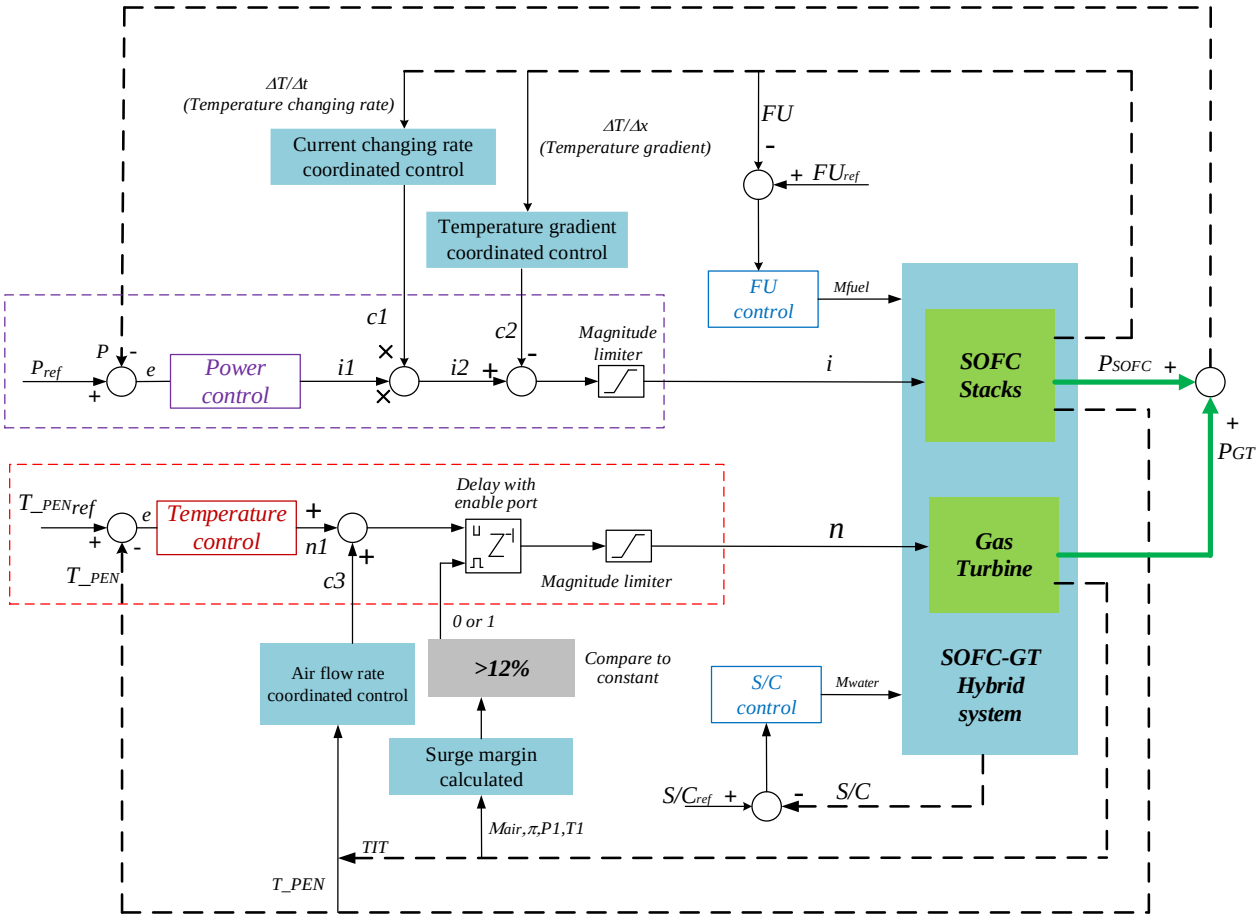


Fig.9. Coordinated control approach of SOFC-GT

- Current changing rate coordinated (CCRC) control: Because the rapid or big change in current may result in the temperature changing rate inside fuel cell close to or even higher than the boundary value, leading to cell breakdown. The CCRC control is used to slow down the transient current changing rate.

In this loop, the signal *c1* in Fig.9 can be self-tuned according to the current safety margin of temperature changing rate (Max. $\Delta T/\Delta t$) inside fuel cell stacks.

$$c1(t)=f_1(\mathrm{Max}.\frac{\Delta T}{\Delta t}(t),\mathrm{Boundary}.\frac{\Delta T}{\Delta t})\begin{cases} if:\mathrm{Max}.\frac{\Delta T}{\Delta t}(t)\ \ \mathrm{Boundary}.\frac{\Delta T}{\Delta t},\ c1(t)=1 \\ if:\mathrm{Max}.\frac{\Delta T}{\Delta t}(t)\ \text{is close to}\ \mathrm{Boundary}.\frac{\Delta T}{\Delta t},\ 0<c1(t)<1 \end{cases} \tag{20}$$

- Temperature gradient coordinated (TGC) control: Generally, the temperature gradient inside fuel cell stacks is mainly related with the local current density. A higher local current density may lead to the temperature gradient exceeds the material limit. Therefore, the TGC control is performed to reduce the current overshoot in transient process.

In this loop, the signal *c2* in Fig.9 can be self-tuned according to the current safety margin of temperature gradient (Max. $\Delta T/\Delta x$) at PEN structure.

$$c2(t) = f_2(\mathrm{Max}.\frac{\Delta T}{\Delta x}(t), \mathrm{Boundary}.\frac{\Delta T}{\Delta x}) \begin{cases} if: \mathrm{Max}.\frac{\Delta T}{\Delta x}(t) \ \square \ \mathrm{Boundary}.\frac{\Delta T}{\Delta x},\ c2(t) = 0 \\ if: \mathrm{Max}.\frac{\Delta T}{\Delta x}(t) \text{ is close to } \mathrm{Boundary}.\frac{\Delta T}{\Delta x},\ 0 < c2(t) < i2 \end{cases} \tag{21}$$

Where, $i2$ is the signal of current before tuned by TGC control.

- Air flow rate coordinated (AFRC) control: Although a reasonable temperature at PEN structure ($T_{\mathrm{PEN}}$) at final state can be obtained by the temperature control, which does not ensure the temperature is always in the expected ranges due to the fluctuation of the transient behavior. Therefore, the AFRC control is given to reduce the fluctuation of temperature in transient process by regulating the air flow rate.

In this loop, the signal *c3* in Fig.9 can be self-tuned according to the current safety margin of $T_{\mathrm{PEN}}$ and TIT (turbine inlet temperature). Which is an auxiliary signal to manipulate the micro gas turbine rotate speed.

$$c3(t) = f_3(T_{PEN}(t), \mathrm{Boundary}.T_{PEN}, TIT(t), \mathrm{Boundary}.T_{TIT}) \begin{cases} if: T_{PEN}(t)\ \&TIT(t) \ \square \ \text{Boundery values: } c3(t) = 0 \\ Else: 0 < c3(t) < n1 \end{cases} \tag{22}$$

Where, $n1$ is the signal of rotate speed before tuned by AFRC control.

- Surge margin coordinated (SMC) control: A minimum 12% surge margin must be ensured to protect the healthy operation of compressor. For a micro gas turbine, a reasonable operation state can avoid compressor surge phenomenon occurs effectively. The SMC control loop consists of a surge margin calculated block, a compare to constant block and a delay block with enable port. The surge margin of compressor cannot be measured directly, which can be calculated as:

$$SM = \frac{\pi_{surge}(\frac{m_a\sqrt{T_1}}{P_1})_{work}}{\pi_{work}(\frac{m_a\sqrt{T_1}}{P_1})_{surge}} - 1 \tag{23}$$

where, $\pi$ $m_a$ $T_1$ $P_1$ are pressure ratio, air flow rate, inlet temperature and pressure of compressor.

In the delay block of this loop, when the input of port is 1, this block is regarded as enabled; when the input is 0, this block is regarded as disabled. For continuous enable signals, the block takes the last state of the input signal. And if the block becomes disabled after being enabled, the module does not execute and maintains its final value. Therefore, the surge margin of compressor can be monitored and maintained above 12% in the whole process.

## 5. Results and Discussions

### 5.1 Determine the set point of temperature

This work adjusted the fuel cell stacks current and air flow rate to control output power and SOFC working temperature and regulating the fuel flow rate and water flow rate to maintain the FU and S/C constant. While the load of SOFC-GT is changed, a reasonable set point of temperature in temperature controller can obtain the better

trade-off between system performance and safe dynamic operation of SOFC-GT. In order to find an optimal set point of temperature, the performance of SOFC-GT hybrid system effected by the current and air flow rate at steady state are investigated. And the variation of system output power and electrical efficiency with various current and air flow rate are given in Fig.10 and Fig.11 respectively. Although the increase in system power and efficiency show in the fuel cell thermal crack may occur while a relatively higher current is given. Meanwhile, this work selects the maximum temperature inside fuel stacks as the control variable. And the variation of the maximum temperature at PEN structure (Max.$T_{PEN}$) in various current and air flow rate is given in fig.12.

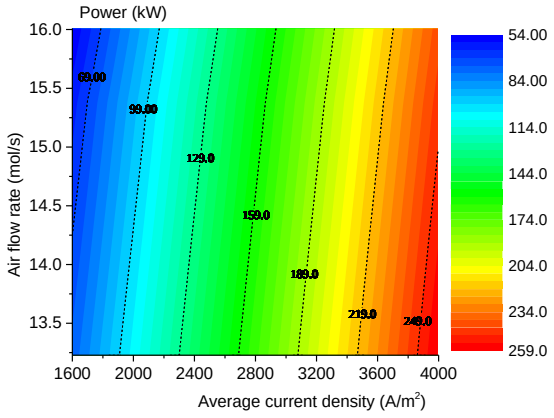


Fig.10. Variation ranges of system output power

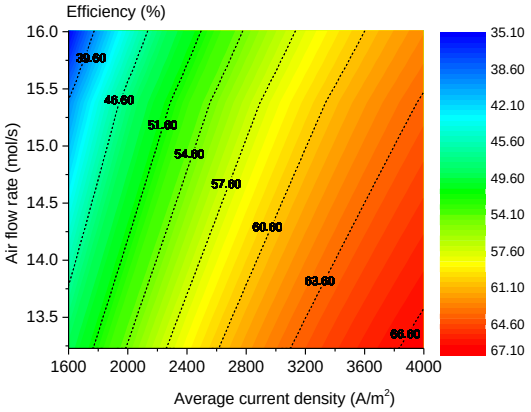


Fig.11. Variation ranges of system efficiency

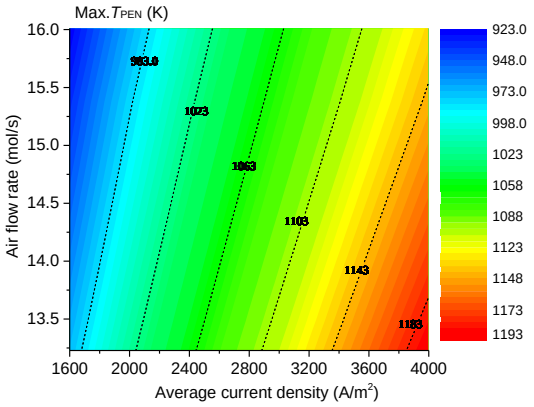


Fig.12. Variation ranges of Max.$T_{PEN}$

Clearly, adjusting current and air flow rate simultaneously allow the system gains with better performance over a wide temperature range. A reasonable temperature is important to balance the efficiency and safe operation of SOFC-GT, and the variation ranges of power, efficiency and temperature are meaningful to determine the set point of temperature for temperature controller. The variation of temperature set point in different SOFC-GT output power is given in fig.13. While the output power of SOFC-GT is 180kW, the minimum temperature set point of 1078K is necessary to make the electrical efficiency of SOFC-GT higher than 60%, and this figure is 1093K to

make the electrical efficiency of SOFC-GT higher than 61%. In addition, while the power of 242 kW (Designed power) is produced, the minimum temperature set point of 1133K is necessary to ensure the efficiency of SOFC-GT is higher than 60%.

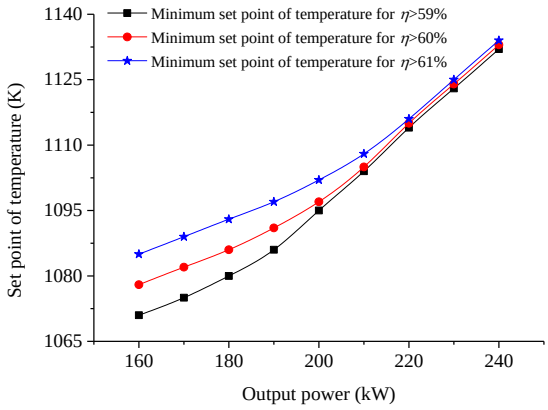


Fig.13. The minimum set point of temperature in different output power and efficiency

## 5.2 Load step-down operation

### 5.2.1 Control strategy designed

The aim of this work is to achieve fast load following, healthy thermal management and safe operation of SOFC-GT by the proposed coordinated control approach. In order to obtain the optimal transient behavior in load step-down operation, four methods are designed by combining different coordinated protection loops during the load step-change from the designed value (242kW) to 180kW. The different parameters set in each of the four cases are given in Table.2.

Table.2. Comparison among four control methods in load step-down operation of SOFC-GT

| Case | 1 | 2 | 3 | 4 |
|---|---|---|---|---|
| Power control | ✓ | ✓ | ✓ | ✓ |
| Set point of power | 180kW | 180kW | 180kW | 180kW |
| Temperature control | × | × | ✓ | ✓ |
| Set point of temperature | - | - | **1090K** | **1100k** |
| Fuel utilization control | ✓ | ✓ | ✓ | ✓ |
| Set point of FU | 75% | 75% | 75% | 75% |
| Steam to carbon control | ✓ | ✓ | ✓ | ✓ |
| Set point of S/C | 2 | 2 | 2 | 2 |
| Current changing rate coordinated control | × | ✓ | ✓ | ✓ |
| Temperature gradient coordinated control | ✓ | ✓ | ✓ | ✓ |
| Air flow rate coordinated control | × | × | ✓ | ✓ |
| Surge margin coordinated control | ✓ | ✓ | ✓ | ✓ |

| | | | | |
|---|---|---|---|---|
| Magnitude limiter of current | ✓ | ✓ | ✓ | ✓ |
| Magnitude limiter of MGT rotate speed | ✓ | ✓ | ✓ | ✓ |

In case1 there is no temperature control and there is the current changing rate coordinated control (CCRC). Case2 is with CCRC but without temperature control. Case3 and Case4 are considered with CCRC and temperature control together. In addition, Case3 and Case4 have different set point in temperature controller, 1090K and 1100K respectively. The FU and S/C are always controlled as 75% and 2 respectively. Besides that, the surge margin coordinated control is conducted to keep the surge margin of compressor greater than 12% in the whole transient process. Also, two magnitude limiters are used in this four cases to ensure the current and MGT rotate speed are in the acceptable ranges.

### 5.2.2 Transient performance investigation in different control strategies

Fig.14-Fig.15 show the transient behavior of power and efficiency of SOFC-GT in these four cases. It can be observed that the transient behaviors of SOFC-GT are totally different in different control methods. The efficiency of SOFC-GT hybrid system at final state are 58.18%, 58.18%, 60.31% and 61.61% in case 1-4 respectively. Although the case1 can obtain the shortest response time, it fails in improving the efficiency of SOFC-GT. The maximum efficiency of SOFC-GT is gained in case4 (Fig. 15). This is because that the working temperature of SOFC in case 4 is highest compared with the other three cases, and the rise in SOFC working temperature causes the improve in system performance. Results concluded that the better trade-off between fuel cell thermal management and system efficiency can be obtained by the temperature control.

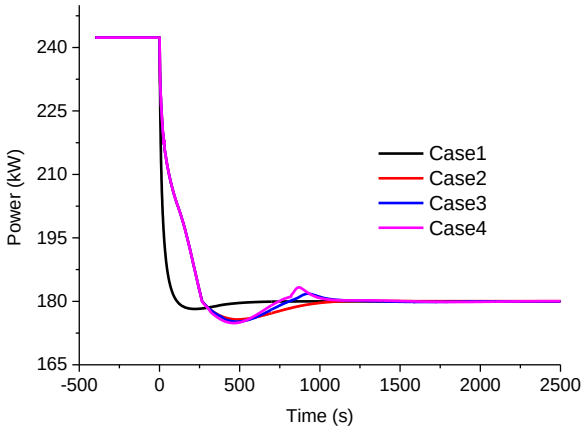


Fig.14. Transient response of system power

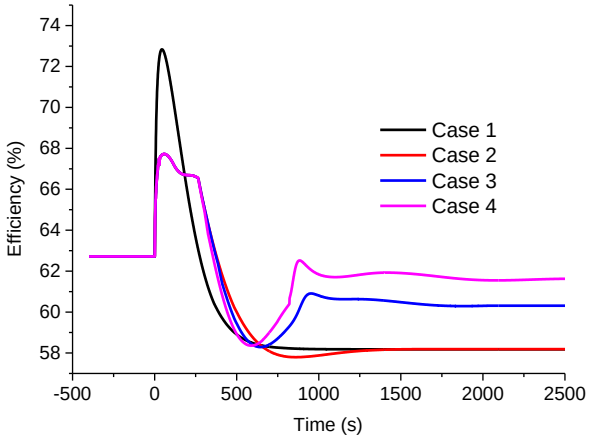


Fig.15. Transient response of system efficiency

Fig.16-fig.17 give the transient responses of average current density and fuel cell potential. It has been observed that the average current density at final state in case4 and case3 are 3085A/m$^2$ and 3020A/m$^2$ respectively. Meanwhile, the cell potential at final state in case4 and case3 are 0.637V and 0.605V respectively. While the hybrid

SOFC-GT system operation in case4, a smaller air flow rate is gained to achieve the fuel cell working in a higher temperature. In addition, the current overshoot in case1-4 are 18.2%, 12.6%, 9.3% and 7.4% respectively. The results shown that the current overshoot is decreased significantly (almost by 10.8%) while the temperature control and current changing rate coordinated control are enabled together.

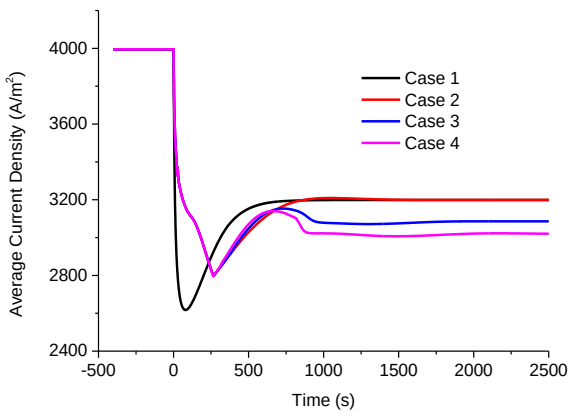


Fig.16. Transient response of fuel flow rate

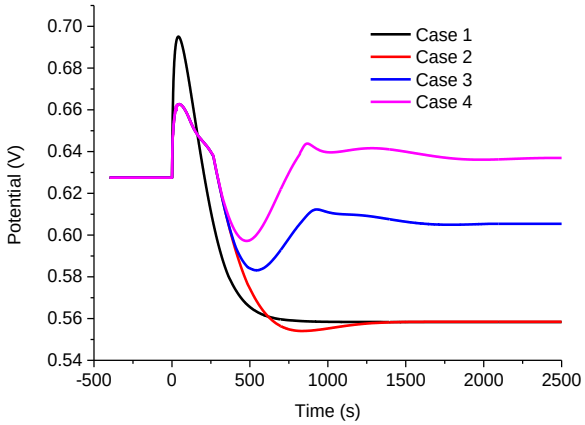


Fig.17. Transient response of cell potential

The temperature inside fuel cell is not uniform. Fig.18 gives the transient behavior of the temperature distribution at PEN structure along flow direction in these four cases. It can be seen that the temperature gradient and temperature changing rate in different position are different. Overall, the temperature at PEN structure ($T_{PEN}$) shown an increasing trend along the flow direction. And the $T_{PEN}$ at the final state is smaller than that in the initial state at the same position. By comparing, we can found that the distribution of $T_{PEN}$ is relatively smooth in case4. Also, relatively high temperature is concentrated at the outlet of fuel cell stacks (around the dimensionless axial position of 0.8-1 along the flow direction).

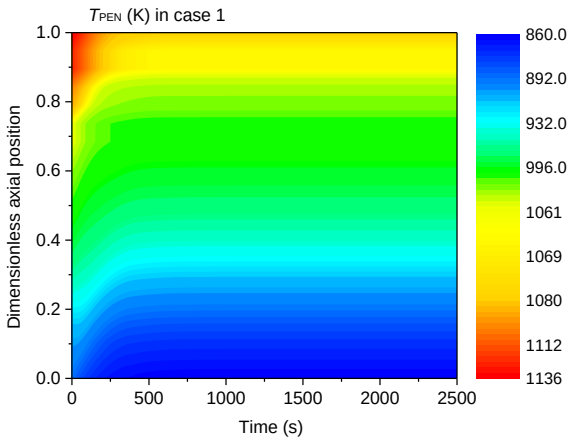


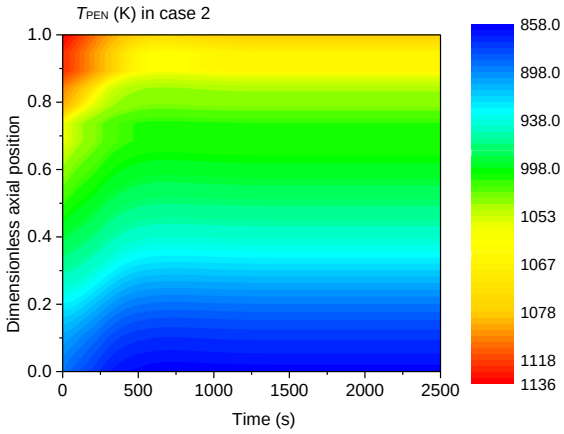

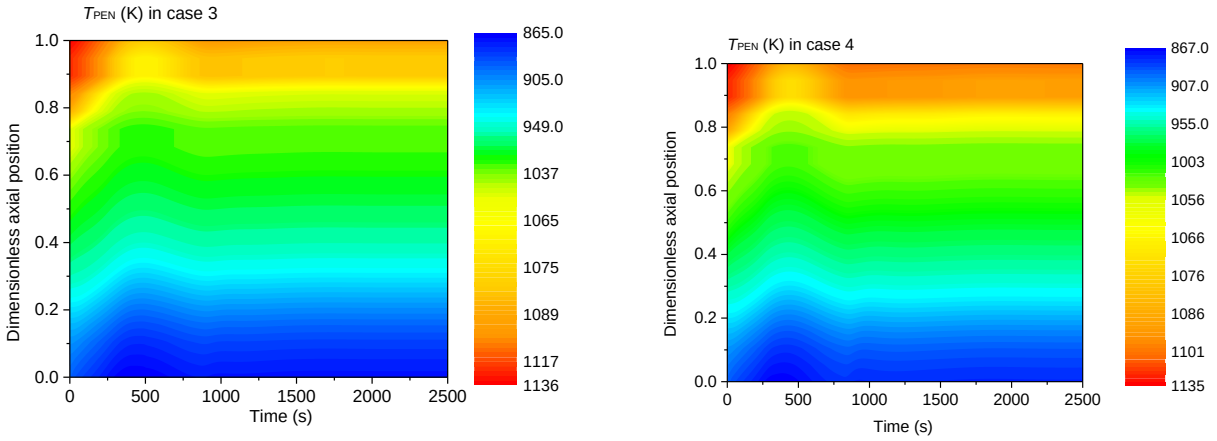


Fig.18. Transient behavior of $T_{PEN}$ along flow direction

Generally, the maximum temperature of PEN structure (Max.$T_{PEN}$) occurs at the end of SOFC. Fig.19 represents the transient response of Max.$T_{PEN}$. Although the case1 is the quickest strategy to achieve thermal equilibrium within the fuel cell, which results in the excessive temperature changing rate. Fig.20 describes the transient response of maximum temperature gradient (Max.$\Delta T/\Delta x$) and temperature changing rate (Max.$\Delta T/\Delta t$) at PEN structure. The transient Max.$\Delta T/\Delta t$ is almost 0.3K/s while the current changing rate coordinated (CCRC) control is not enabled (case1), which will cause the excessive thermal stresses within the fuel cell, and damage the SOFC permanently. And the figure can be decreased to 0.157K/s while the CCRC control is started, which causes the transient maximum temperature changing rate decreased by almost 47.7%. Although case1 is more simply and quickly than others, it is not suggested in load big changes operation for safety reasons. It also can be seen from fig.20 that the Max.$\Delta T/\Delta x$ at final state in case4 (7.49K/cm) is slightly higher than that in case3 (7.33 K/cm).

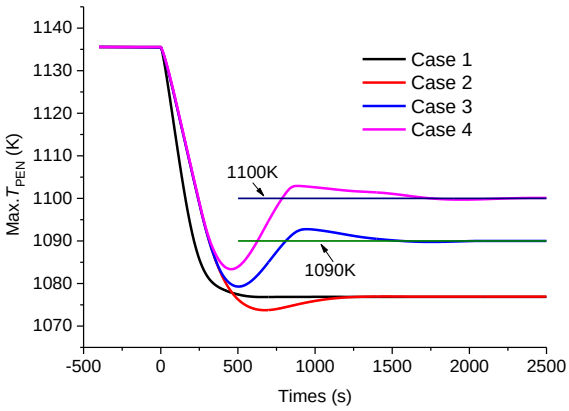


Fig.19. Transient response of Max.$T_{PEN}$

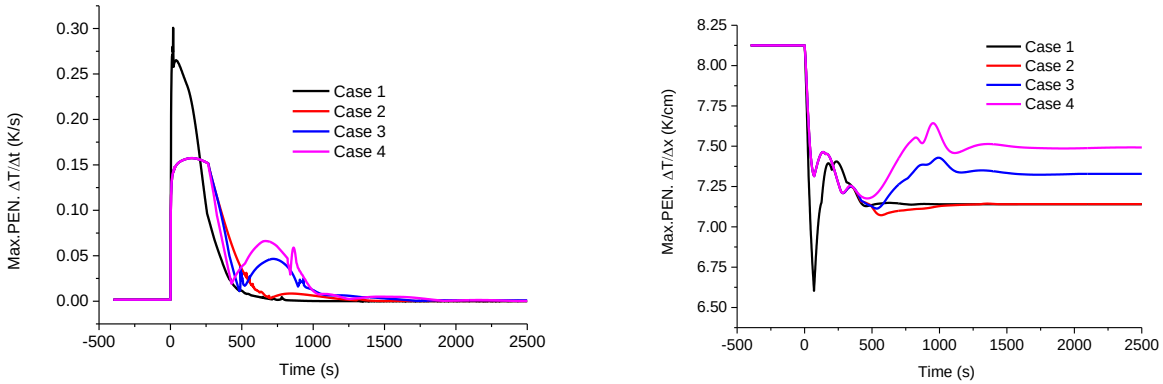


Fig.20. Transient response of Max.$\Delta T/\Delta x$ and Max.$\Delta T/\Delta t$ at PEN structure

In addition, the turbine inlet temperature (TIT) is a key parameter to influence the output power and system performance. Which is mainly determined by the air flow rate, fuel flow rate and fuel utilization inside fuel cell stacks. The transient behavior of TIT is shown in Fig.21. Clearly, the highest TIT of 1085K at finally state is obtained in case4 operation, and the maximum overshoot of TIT is 5.41% in this strategy.

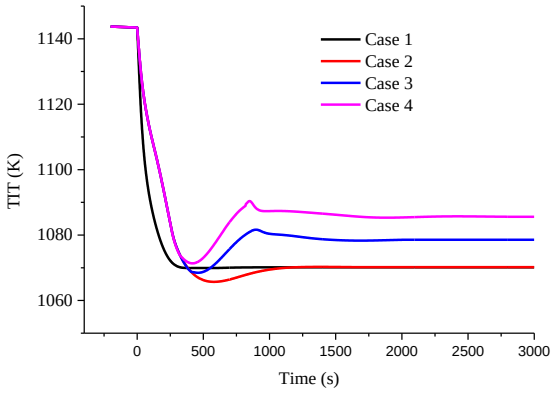


Fig.21. Transient response of TIT

Through the above analysis, we can concluded that the case4 can obtain a best trade-off between system performance and safe dynamic operation of SOFC-GT during load step decrease. In addition, the reasonable compressor surge margin (SM) is also necessary to ensure the high efficient and reliable operation of gas turbine. And the dynamic response of SM in case4 is given in Fig.22. The surge margin is directly depended on the working state of compressor. We can clearly found that the surge margin of compressor is always maintained greater than 12% by the surge margin coordinated control. In addition, the transient behavior of power split between SOFC and MGT is also given in Fig.22. The power ratio between SOFC and GT ($P_{SOFC}/P_{GT}$) is firstly increase and then fluctuate to steady state during the time. Generally, the power ratio is influenced by various strongly coupled parameters together. The gas turbine output power is mainly effected by the rotate speed, turbine inlet temperature and fuel flow rate. The output power of SOFC is mainly depended on the current in fuel cell stacks, fuel utilization

and working temperature.

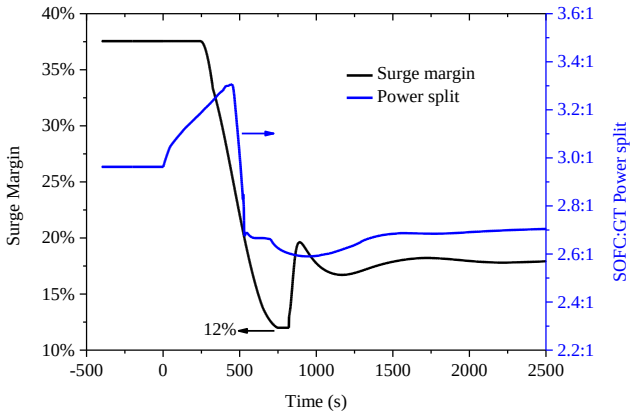


Fig.22. Transient response of surge margin and power split

## 5.3 Load step-up operation

### 5.3.1 Control strategy designed

In the previous section, the results concluded that a coordinated control of power, temperature, FU, S/C, CCRC and SMC can make the hybrid system gains optimal during load step-down operation. However, in the load step-up operation of SOFC-GT, the changing trends of key parameters, such as fuel flow rate, temperature distribution and temperature gradient inside fuel cell stacks, are totally different with that in load step-down operation. Thus, the control strategy must be redesigned in load step-up operation for obtaining the optimal control effect. And three control methods are given while the load step-change from 180kW to 242kW (Designed value). The different among these three cases are listed in Table.3.

Table.3. Comparison among three control modes in load step-up operation of SOFC-GT

| Case | A | B | C |
|---|---|---|---|
| Power control | ✓ | ✓ | ✓ |
| Set point of power | 242kW | 242kW | 242kW |
| Temperature control | ✓ | ✓ | ✓ |
| Set point of temperature | 1140K | 1140K | 1140K |
| Fuel utilization control | ✓ | ✓ | ✓ |
| Set point of FU | 75% | 75% | 75% |
| Steam to carbon control | ✓ | ✓ | ✓ |
| Set point of S/C | 2 | 2 | 2 |
| Current changing rate coordinated control | ✓ | ✓ | ✓ |
| Temperature gradient coordinated control | × | × | ✓ |
| Air flow rate coordinated control | × | ✓ | ✓ |
| Surge margin coordinated control | ✓ | ✓ | ✓ |

| | | | |
|---|---|---|---|
| Magnitude limiter of current | ✓ | ✓ | ✓ |
| Magnitude limiter of MGT rotate speed | ✓ | ✓ | ✓ |

Case A considers no temperature gradient coordinated (TGC) control and no air flow rate coordinated (AFRC) control. Case B has AFRC, while case C have both two loops. Besides that, the control structure is the same with the load step-down operation, including power control, temperature control, fuel utilization control, steam to carbon control, current changing rate coordinated (CCRC) control and surge margin coordinated (SMC) control. Also, two magnitude limiter are used to prevent the performances of SOFC-GT deviate too much from the expected ranges during transient operation.

### 5.3.2 Transient performance investigation in different control strategies

Fig.23 show the transient behavior of maximum PEN structure temperature (Max.$T_{PEN}$) in these three cases. The transient Max.$T_{PEN}$ are 1165K, 1157K and 1152K in case A, B and C respectively. Results indicate that the AFRC and TGC coordinated control (Case C) are effectively to reduce the fluctuating of SOFC working temperature, which results in the temperature overshoot reduced from 2.28% to 1.12%.

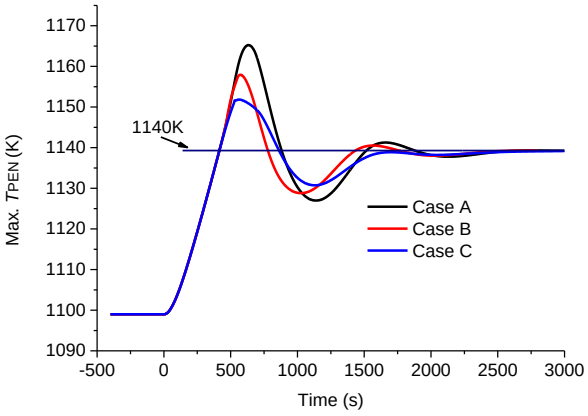


Fig.23. Transient response of Max.$T_{PEN}$

Fig.24 give the transient response of maximum temperature gradient (Max.$\Delta T/\Delta x$) at PEN structure. The results show that the case C can decrease the transient maximum temperature gradient significantly, which causes the transient Max.$\Delta T/\Delta x$ decrease by almost 0.18K/cm. Because Case C can reduce the fluctuations of system effectively, which is generally suggested for SOFC-GT hybrid system in load step-up operation. f

Fig.25 gives the transient behavior of the temperature distribution at PEN structure along flow direction in case C. It was observed that the $T_{PEN}$ (temperature at PEN structure) at the final state is smaller than that in the initial state at the same position, and relatively high temperature is concentrated at the outlet of fuel cell stacks (around the dimensionless axial position of 0.8-1 along the flow direction).

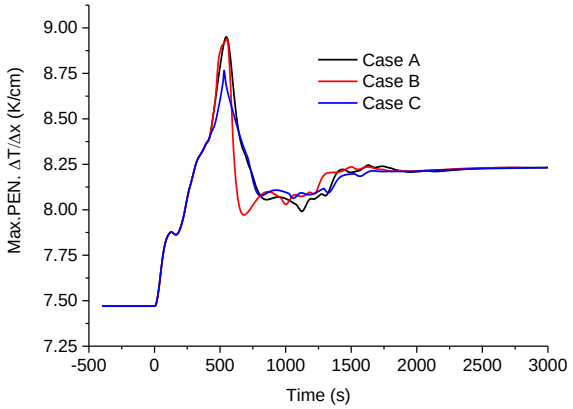


Fig.24. Transient response of Max.$\Delta T/\Delta x$ at PEN structure

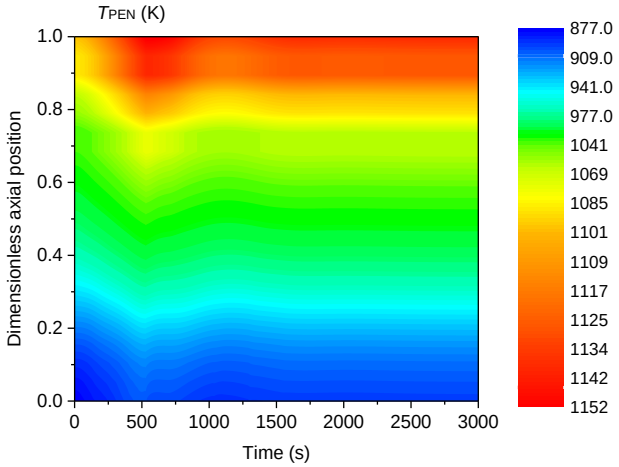


Fig.25. Transient behavior of $T_{PEN}$ along flow direction in case C

In addition, the transient behavior of turbine inlet temperature is given in Fig.26. It was observed that fluctuation of TIT is similar in this three cases. The maximum TIT in transient process are 1176K, 1179K and 1169K in case A, B and C respectively. Also, the maximum overshoot of TIT is decreased from 2.74% to 2.16% while case C is conducted.

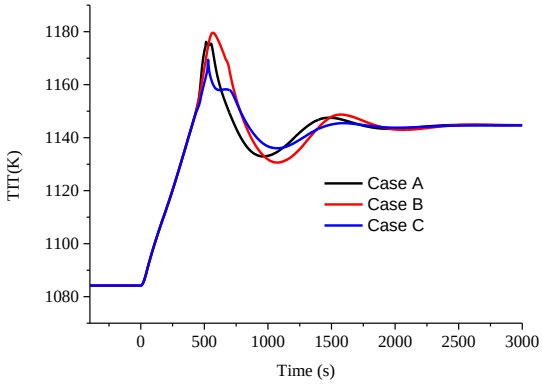


Fig.26. Transient response of TIT

Through the above analysis, we can easily found that the control strategy of case C (which with power control, temperature control, FU control, S/C control and the coordinated control of CCRC, TGC, AFRC and SMC together) can obtain the best trade-off between system performance and safe dynamic operation of SOFC-GT during load step increase. While the control system is operated in case C, the transient behavior in compressor surge margin and SOFC:GT power split is given in Fig.27. Generally, the compressor surge margin has a direct relationship with rotate speed of MGT. And a highest surge margin of 37.56% is constrained by the upper limit of rotate speed. Also, the power ratio between SOFC and GT ($P_{SOFC}/P_{GT}$) is firstly increase and then fluctuate to steady state during the time, almost 74% of the power is supplied by SOFC at the finally state.

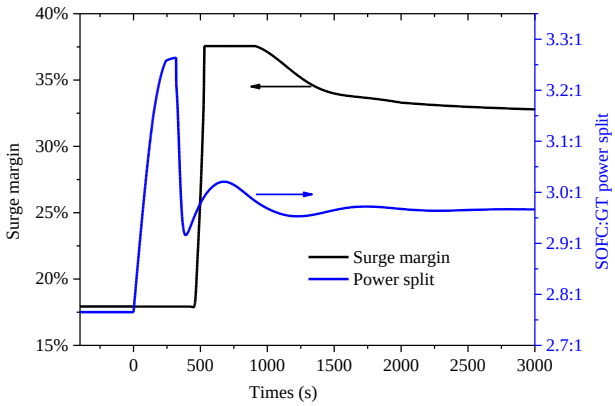


Fig.27. Transient response of SM and power split in case C

While the control system is operated in case C, the transient response of average current density and output power of SOFC-GT are given in Fig.28. The average current density and output power of SOFC-GT at final state are 3912A/m$^2$ and 242kW respectively. In this condition, the hybrid system gains 63.38% efficiency at the finally state.

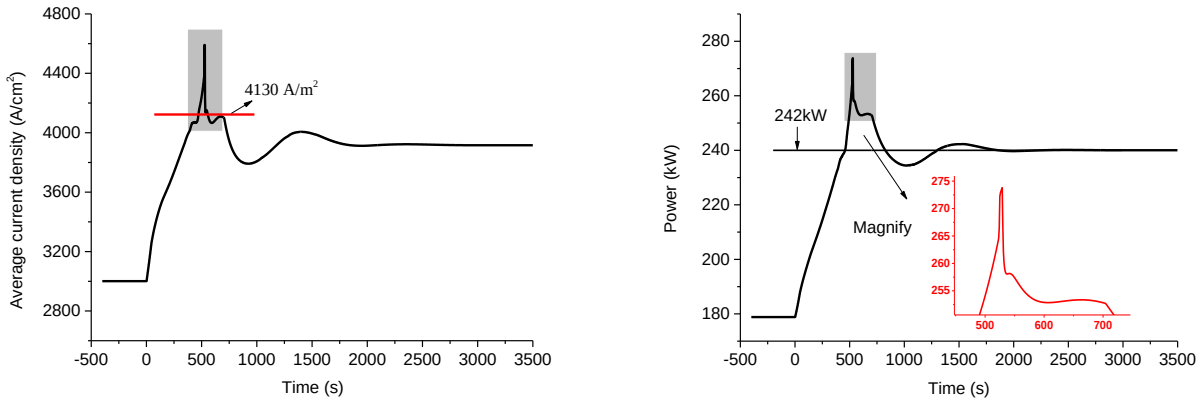


Fig.28. Transient response of average current density and output power of SOFC-GT

It also can be seen that the performance of SOFC-GT showing a large fluctuation during 500s to 550s. This is because that the temperature gradient coordinated control causes a large fluctuation in transient current of SOFC, and this situation can be prevented efficiently by set the reasonable upper limit value of current in magnitude limiter.

Fig.28 suggested that the performance fluctuation could be prevent efficiently while the upper limit of average current density is set as around 4130A/m$^2$. Fig.29 compares the transient response of current, output power and maximum temperature gradient (Max.$\Delta T/\Delta x$) in the condition of current magnitude limiter is started. Results indicate that, while 4130A/m$^2$ of average current density is set as the upper limit, the power overshoot decreases from 14.1% to 7.1% and the current overshoot is reduced from 17.2% to 5.6%. In addition, the transient Max.$\Delta T/\Delta x$ at PEN structure is reduced by 0.13K/cm.

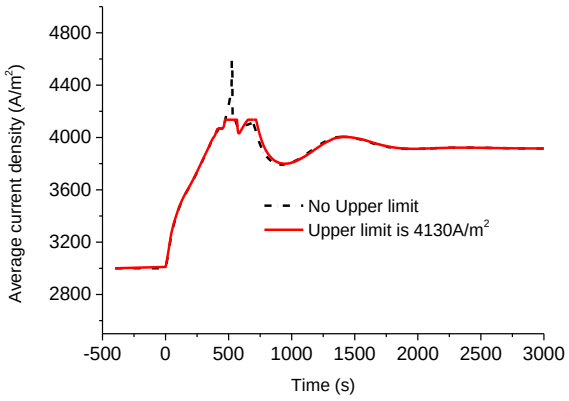


(a)

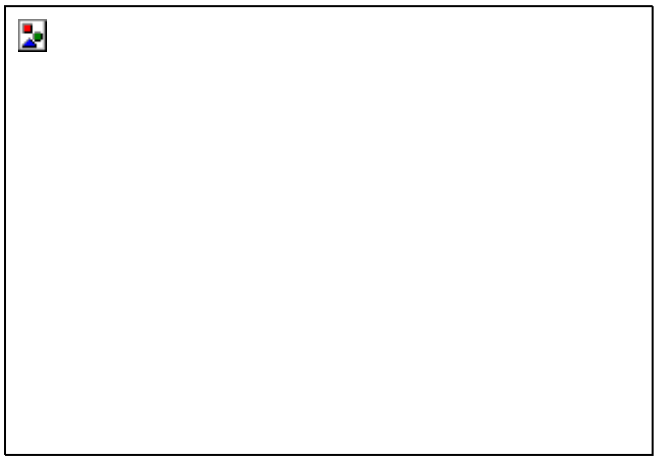

(b)

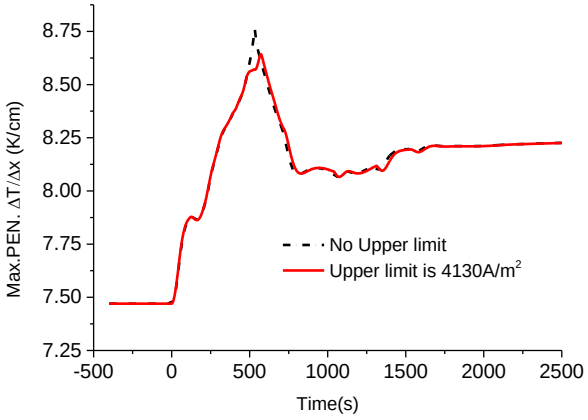


(c)

Fig.29. Transient behavior of SOFC-GT. (a) Average current density; (b)Output power;

(c) Max.$\Delta T/\Delta x$ at PEN structure

## 6. Conclusion

A novel control approach combining the multi control loops with the coordinated protection loops is proposed in this work to improve the transient performance of SOFC-GT in the process of load following. The fuzzy-PID control is developed to meet the control requirements of the nonlinear time varying SOFC-GT hybrid system. The control system regulates the output power, SOFC working temperature, fuel utilization and steam to carbon ratio by

manipulating the variables, such as fuel flow rate, water flow rate, micro gas turbine rotate speed and fuel cell stacks current. In addition, the coordinated protection loops are designed to eliminate the instability and ensure the safety operation of SOFC-GT. The main results are listed as follow:

1) A 242kW SOFC-GT hybrid system fueled by methane is designed in this work. The variation in output power, electrical efficiency and maximum temperature at PEN structure are investigated, which can give instructions to determine the set point of temperature for temperature controller. The results show that, while the output power of SOFC-GT is 180kW, the minimum temperature set point of 1078K is necessary to make the electrical efficiency of SOFC-GT higher than 60%. At a set point temperature of 1093K the electrical efficiency of SOFC-GT is higher than 61%.

2) During the load step-down operation of SOFC-GT, the results show that the current overshoot decreases significantly (almost by 10.8%) while the temperature control and current changing rate coordinated (CCRC) control are enabled together. Meanwhile, while the load of SOFC-GT step-change from the designed value (242kW) to 180kW, the transient Max.$\Delta T/\Delta t$ is almost 0.3K/s while the current changing rate coordinated control is not enabled, which will cause the excessive thermal stresses within fuel cell stacks, and damage the SOFC permanently. And the figure can be decreased to 0.157K/s while the CCRC control is started, which causes the transient maximum temperature changing rate decreased by almost 47.7%.

3) The results also concluded that the temperature overshoot has been reduced from 2.28% to 1.12% while the air flow rate coordinated control and temperature gradient coordinated control are enabled together in the load step-up operation of SOFC-GT. Meanwhile, this control strategy leads to the transient Max.$\Delta T/\Delta x$ decrease by 0.18K/cm while the load step-change from 180kW to 242kW (designed value). In addition, a reasonable upper limit in current magnitude limiter can improve the transient behavior of SOFC-GT significantly. While 4130A/m$^2$ of average current density is set as the upper limit, the power overshoot is decreased from 14.1% to 7.1%, the current overshoot is reduced from 17.2% to 5.6%. Meanwhile, the transient Max.$\Delta T/\Delta x$ is reduced by 0.13K/cm.

## Acknowledgements

The research is supported by National Natural Science Foundation of China under Grant No. 51806137, and Shanghai Rising- Star Program under Grant No. 20QA1404700.

## References

[1] EIA. International energy outlook 2019 [R]. US Energy Information Administration (EIA), 2019.

[2] Zabihian F, Fung A S. Performance analysis of hybrid solid oxide fuel cell and gas turbine cycle: Application of alternative fuels[J]. Energy Conversion & Management, 2013, 76:571-580.

[3] Buonomano A, Calise F, d'Accadia MD, et al. Hybrid solid oxide fuel cells-gas turbine systems for combined

heat and power: a review[J]. Applied Energy 2015;156: 32-85.
[4] Huang Y, Turan A. Mechanical equilibrium operation integrated modelling of hybrid SOFC – GT systems: Design analyses and off-design optimization[J]. Energy, 2020, 208:118334.
[5] Ghorbani S, Manesh M, Nourpour M, et al. Exergoeconomic and exergoenvironmental analyses of an integrated SOFC-GT-ORC hybrid system[J]. Energy, 2020, 206:118151.
[6] Chan S H, Ho H K, Tian Y. Modelling of simple hybrid solid oxide fuel cell and gas turbine power plant[J]. Journal of Power Sources, 2002, 109(1):111-120.
[7] Saebea D, Authayanun S, Patcharavorachot Y, e al. Effect of anode–cathode exhaust gas recirculation on energy recuperation in a solid oxide fuel cell-gas turbine hybrid power system[J]. Energy, 2016, 94:218-232.
[8] Maghsoudi P, Sadeghi S. A novel economic analysis and multi-objective optimization of a 200-kW recuperated micro gas turbine considering cycle thermal efficiency and discounted payback period[J]. Applied Thermal Engineering, 166:114644.
[9] Zeng Z , Qian Y , Zhang Y , et al. A review of heat transfer and thermal management methods for temperature gradient reduction in solid oxide fuel cell (SOFC) stacks[J]. Applied Energy, 2020, 280:115899.
[10] Wasajja, H, Lindeboom, P E F , et al. Techno-economic review of biogas cleaning technologies for small scale off-grid solid oxide fuel cell applications[J]. Fuel Processing Technology, 197:106215.
[11] Azizi M A, Brouwer J. Progress in solid oxide fuel cell-gas turbine hybrid power systems: System design and analysis, transient operation, controls and optimization[J]. Applied Energy, 2018, 215:237-289.
[12] Bao C, Wang Y, Feng D, et al. Macroscopic modeling of solid oxide fuel cell (SOFC) and model-based control of SOFC and gas turbine hybrid system[J]. Progress in Energy and Combustion Science, 2018, 66:83-140.
[13] Komatsu Y, Kimijima S, Szmyd J S. Performance analysis for the part-load operation of a solid oxide fuel cell–micro gas turbine hybrid system[J]. Energy, 2010, 35(2):982-988.
[14] Mclarty D, Brouwer J, Samuelsen S. Fuel cell–gas turbine hybrid system design part II: Dynamics and control[J]. Journal of Power Sources, 2014, 254:126-136.
[15] Akkaya A V, Sahin B, Erdem H H . An analysis of SOFC/GT CHP system based on exergetic performance criteria[J]. International Journal of Hydrogen Energy, 2008, 33(10):2566-2577.
[16] Danylo O, Farida H N, David T, et al. Fuel utilization effects on system efficiency in solid oxide fuel cell gas turbine hybrid systems[J]. Applied Energy, 2018, 228:1953-1965.
[17] Kandepu R, Imsland L, Foss B A, et al. Modeling and control of a SOFC-GT-based autonomous power system[J]. Energy, 2007, 32(4):406-417.
[18] Ferrari, Mario L. Advanced control approach for hybrid systems based on solid oxide fuel cells[J]. Applied Energy, 2015, 145:364-373.
[19] Chen J, Liang M, Zhang H, et al. Study on control strategy for a SOFC-GT hybrid system with anode and cathode recirculation loops [J]. International Journal of Hydrogen Energy, 2017,42(49), 29422-29432
[20] Gheisarnejad, Meysam. An effective hybrid harmony search and cuckoo optimization algorithm based fuzzy PID controller for load frequency control[J]. Applied Soft Computing, 2018, 65:121-138.
[21] Marzooghi H, Raoofat M. Improving the performance of proton exchange membrane and solid oxide fuel cells under voltage flicker using Fuzzy-PI controller[J]. International Journal of Hydrogen Energy, 2012, 37(9):7796-7806.
[22] Cao H, Xi L. Thermal Management-Oriented Multivariable Robust Control of a kW-Scale Solid Oxide Fuel Cell Stand-Alone System[J]. IEEE Transactions on Energy Conversion, 2016, 31(2):1-10.
[23] Wu X J , Zhu X J . Multi-loop control strategy of a solid oxide fuel cell and micro gas turbine hybrid system[J]. Journal of Power Sources, 2011, 196(20):8444-8449.
[24] Gandiglio M, Lanzini A, Leone P, et al. Thermoeconomic analysis of large solid oxide fuel cell plants: Atmospheric vs. pressurized performance[J]. Energy, 2013, 55:142–155.
[25] Be A , Ac B , Jh A , et al. Thermo-environmental and economic comparison of three different arrangements of

solid oxide fuel cell-gas turbine (SOFC-GT) hybrid systems[J]. Energy Conversion and Management, 2018, 168:343-356.

[26] Traverso A , Magistri L , AF Massardo. Turbomachinery for the air management and energy recovery in fuel cell gas turbine hybrid systems[J]. Energy, 2010, 35(2):764-777.

[27] Consultant RBS. Advancing Europe's energy systems: stationary fuel cells in distributed generation. In: Union LPOotE, editor; 2015.

[28] Lv X, Lu C, Wang Y, et al. Effect of operating parameters on a hybrid system of intermediate-temperature solid oxide fuel cell and gas turbine[J]. Energy, 2015, 91:10-19.

[29] Lv X , Gu C , Liu X , et al. Effect of gasified biomass fuel on load characteristics of an intermediate-temperature solid oxide fuel cell and gas turbine hybrid system[J]. International Journal of Hydrogen Energy, 2016, 41 ( 22):9563-9576.

[30] Lv X, Liu X, Gu C, et al. Determination of safe operation zone for an intermediate-temperature solid oxide fuel cell and gas turbine hybrid system[J]. Energy, 2016, 99:91-102.

[31] Wang X, Lv X, Weng Y. Performance analysis of a biogas-fueled SOFC/GT hybrid system integrated with anode-combustor exhaust gas recirculation loops[J]. Energy, 2020, 197:117213.

[32] Luo X J, Fong K F. Development of 2D dynamic model for hydrogen-fed and methane-fed solid oxide fuel cells[J]. Journal of Power Sources, 2016, 328:91-104.

[33] Jia J, Li Q, Luo M, et al. Effects of gas recycle on performance of solid oxide fuel cell power systems. Energy 2011;36(2):1068-1075.

[34] Aguiar P, Adjiman C S, Brandon N P. Anode-supported intermediate temperature direct internal reforming solid oxide fuel cell. I: model-based steady-state performance[J]. Journal of Power Sources, 2004, 138:120-136.

[35] Aguiar P, Adjiman C S, Brandon N P. Anode-supported intermediate-temperature direct internal reforming solid oxide fuel cell: II. Model-based dynamic performance and control[J]. Journal of Power Sources, 2005, 147:136-147.

[36] Sghaier SF, Khir T, Brahim AB. Energetic and exergetic parametric study of a SOFC-GT hybrid power plant[J]. Int J Hydrogen Energy 2018, (43):3542-3554.

[37] Hosseinpour J, Chitsaz A, Eisavi B, et al. Investigation on performance of an integrated SOFC-Goswami system using wood gasification[J]. Energy 2018;158: 614-628

[38] Patcharavorachot Y, Paengjuntuek W, Assabumrungrat S, et al. Performance evaluation of combined solid oxide fuel cells with different electrolytes[J]. International Journal of Hydrogen Energy, 2010, 35(9):4301-4310.

[39] Badur J, Marcin Lemański, Kowalczyk T, et al. Zero-dimensional robust model of an SOFC with internal reforming for hybrid energy cycles[J]. Energy, 2018, 158:128-138.

[40] Kang Y W, Li J, Cao G Y, et al. A reduced 1D dynamic model of a planar direct internal reforming solid oxide fuel cell for system research[J]. Journal of Power Sources, 2009, 188(1):170-176.

[41] Min G, Park Y J, Hong J. 1D thermodynamic modeling for a solid oxide fuel cell stack and parametric study for its optimal operating conditions[J]. Energy Conversion and Management, 2020, 209:112614.

[42] Achenbach E. Three-dimensional and time-dependent simulation of a planar solid oxide fuel cell stack[J]. Journal of Power Sources, 1994, 49:333-348.

[43] Van Biert L, Godjevac M, Visser K, et al. Dynamic modelling of a direct internal reforming solid oxide fuel cell stack based on single cell experiments[J]. Applied Energy, 2019, 250, 976-990.

[44] Zhao F, Anil V, Virkar. Dependence of polarization in anode-supported solid oxide fuel cells on various cell parameters. J Power Sour 2005;141:79-95

[45] Lv X, Zeng W, Ding X, et al. Experimental investigation of a novel micro gas turbine with flexible switching function for distributed power system[J]. Frontiers in Energy, 2020:1-11.

[46] Chen Q. Research on nonlinear characteristics and coordinated control of MCFC-GT hybrid system[D]. PhD. Shanghai Jiao Tong University; 2007.

[47] Lv X, Ding X, Weng Y. Catalytic combustion of ultra-low heating value fuels over 0.5%Pd/ZrO2/g-Al2O3 catalyst. Hong kong, China, 2018 ICAE, 22-25 august 2018, June 26-30. Charlotte, North Carolina, USA: POWER2017-ICOPE-17; 2017.

[48] Darvish S, Gopalan S, Zhong Y. Thermodynamic Stability Maps for the $La_{0.6}Sr_{0.4}Co_{0.2}Fe_{0.8}O_{3\pm\delta}$–$CO_2$–$O_2$ System for Application in Solid Oxide Fuel Cells[J]. Journal of Power Sources, 2016, 336:351-359.

[49] Jia Z, Sun J, Oh S R, et al. Control of the dual mode operation of generator/motor in SOFC/GT-based APU for extended dynamic capabilities[J]. Journal of Power Sources, 2013, 235:172-180.

[50] Sahu R K, Panda S, Yegireddy N K. A novel hybrid DEPS optimized fuzzy PI/PID controller for load frequency control of multi-area interconnected power systems[J]. Journal of Process Control, 2014, 24(10):1596-1608.

[51] Sahu B K, Nayak J R. A novel hybrid LUS–TLBO optimized fuzzy-PID controller for load frequency control of multi-source power system[J]. International Journal of Electrical Power & Energy Systems, 2015, 74:58-69.

[52] Jin X, Chen K, Ji J, et al. Simulation of hydraulic transplanting robot control system based on fuzzy PID controller[J]. Measurement, 2020, 164:108023.

[53] Stiller C, Thorud B, Bolland O, et al. Control strategy for a solid oxide fuel cell and gas turbine hybrid system[J]. Journal of Power Sources, 2006, 158(1):303-315.

[54] Milewski J, Miller A, Jacek Saaciński. Off-design analysis of SOFC hybrid system[J]. International Journal of Hydrogen Energy, 2007, 32(6):687-698.

[55] Herle J V, Marechal F, Leuenberger S, et al. Process flow model of solid oxide fuel cell system supplied with sewage biogas[J]. Journal of Power Sources, 2004, 131:127-141.